Materials & Design 264 (2026) 115738

Contents lists available at ScienceDirect

Materials & Design

journal homepage: www.elsevier.com/locate/matdes

Effect of nano-SiO_2 content on morphology and performance of PVDF/SiO_2 hybrid membranes: Synergistic enhancement in antifouling and anti-compaction performance

Shuqi Ma [a,1], Fengmei Shi [b,1], Boming Fan [a,1], Qi Shen [a], Jinglong Yuan [a], Chao Lin [a], Yuxin Ma [a,*]

[a] College of Civil Engineering, Heilongjiang University, Harbin 150080, PR China
[b] Heilongjiang Academy of Black Soil Conservation and Utilization, Heilongjiang Academy of Agricultural Sciences, Harbin 150086, PR China

ARTICLE INFO

Keywords:
Membrane fouling
Thermally induced phase separation
Hybrid membrane
SiO_2
Anticompaction

ABSTRACT

Polyvinylidene fluoride (PVDF) membranes suffer from strong hydrophobicity-induced fouling and compaction, limiting their application. Herein, PVDF/SiO_2 hybrid membranes were fabricated via thermally induced phase separation (TIPS) to investigate the effects of nano-SiO_2 content (0–6 wt%) on their morphology and performance. Results showed that SiO_2 incorporation significantly improved hydrophilicity (contact angle reduced from 107.9° to 92.5°) , increased porosity by 14.5% (58.8%→67.3%) and improved pure water flux by 231.5% (from 63.4 w to 210.2 $L{\cdot}m^{-2}{\cdot}h^{-1}$ of 3 wt% of SiO_2 dosage). The membranes with 3 wt% dosage of SiO_2 exhibited the smallest, most uniform spherulites, and optimal synergistic enhancement in antifouling and anti-compaction performance with deformation rate of 37.1% (vs. 49.4% for neat PVDF) and > 60% reduction in irreversible fouling resistance. Hermia model confirmed reversible cake layer fouling. Even at 6 wt% SiO_2 (with aggregation), performance remained superior to neat PVDF. This study provides a strategy for designing durable PVDF membranes for high-pressure water treatment.

1. Introduction

Poly(vinylidene fluoride) (PVDF), owing to its excellent chemical stability, thermal stability, and mechanical strength, has become a core material in membrane separation technology with broad application prospects in water treatment and energy storage fields [1]. However, the inherent strong hydrophobicity of PVDF tends to cause adsorption of organic pollutants, proteins, and colloids, leading to severe membrane fouling characterized by flux decline, increased operational pressure, and shortened membrane lifespan [2,3]. Therefore, enhancing the hydrophilicity of PVDF membranes represents a critical research direction for overcoming these bottlenecks[4]. Researchers have developed various modification techniques to improve PVDF membrane hydrophilicity, including surface grafting, physical coating, and polymer blending. Among these methods, the blending approach that incorporates hydrophilic inorganic nanoparticles into the PVDF matrix has attracted significant attention due to its scalable processing and remarkable effectiveness [1]. The polar functional groups (–OH) on the surfaces of nanoparticles such as TiO_2, Al_2O_3, and SiO_2 can enhance membrane surface wettability and reduce foulant adhesion [5–12]. Silica (SiO_2) nanoparticles, in particular, have emerged as highly promising modifiers due to their high specific surface area, tunable surface chemistry, and strong interfacial interactions with PVDF [10]. Studies have demonstrated that the incorporation of SiO_2 can simultaneously improve the water flux, antifouling properties, and mechanical stability of composite membranes. For instance, Ahsani et al. [11] found that PVDF/Ag-SiO_2 membranes prepared by NIPS method exhibited higher pure water flux, low contact angle, remarkable antibacterial and he flux recovery ratio. Senol-Arslan et al. [4] compared the modification effects of PVDF and polysulfone (PSF) membranes, finding that doping with 2 wt% SiO_2 increased the oil rejection rate of PVDF membranes to 94.1% and PSF membranes to 92.2%, while maintaining high separation performance after 10 cycles; Xu et al. [12] utilized casting solutions with lower critical solution temperature (LCST) characteristics combined with non-solvent thermally induced phase separation (NTIPS) to prepare PVDF/SiO_2 composite membranes, achieving structural regulation from

* Corresponding author at: College of Civil Engineering, Heilongjiang University, Xuefu Road 74, Nangang District, Harbin 150080, PR China.
E-mail addresses: 2010055@hlju.edu.cn, oucmyx@126.com (Y. Ma).
[1] These authors contributed equally to this work.

https://doi.org/10.1016/j.matdes.2026.115738
Received 12 December 2025; Received in revised form 26 January 2026; Accepted 25 February 2026
Available online 26 February 2026
0264-1275/© 2026 The Author(s). Published by Elsevier Ltd. This is an open access article under the CC BY-NC license (http://creativecommons.org/licenses/by-nc/4.0/).

finger-like pores to bicontinuous interconnected pores, resulting in a flux exceeding 318 $L{\cdot}m^{-2}{\cdot}h^{-1}{\cdot}bar^{-1}$ for surfactant-containing oil–water emulsions and a rejection rate over 99.2%. Similarly, Amani et al. [13] confirmed that PVDF/SiO_2-Cu nanocomposite membranes had better-developed finger-like bulk pores, thicker sponge-like surface pores, and enhanced antifouling performance and separation efficiency.

In membrane preparation methods, although the non-solvent induced phase separation (NIPS) method is widely applied, the thermally induced phase separation (TIPS) method is more suitable for preparing PVDF-based composite membranes. The TIPS process involves dissolving polymers in high-boiling-point diluents at elevated temperatures, followed by controlled cooling to induce phase separation. The resulting membranes exhibit uniform pore size distribution, high porosity, and excellent mechanical strength, which are critical for their broad applications [6]. Cui et al. [6] first employed the TIPS method to fabricate PVDF/SiO_2 composite membranes, discovering that micron-sized SiO_2 disrupted PVDF spherulite formation, refined the membrane structure, and enhanced both water flux and tensile strength. Xu et al. [12] further proposed the NTIPS method, which enables flexible customization of membrane pore structures through regulation of PVDF concentration, SiO_2/PVDF mass ratio, and coagulation temperature, thereby providing a novel pathway for the preparation of high-performance membranes. Liang et al. [14] combined TIPS with an in situ sol–gel method to prepare composite membranes, reducing the contact angle from 131° to 101° and significantly improving water flux; Liu et al. [15] and Boateng et al. [16] further demonstrated that the TIPS method enables the fabrication of structurally tunable PVDF/SiO_2 membranes, which exhibited excellent ionic conductivity and thermal stability when used as separators in lithium-ion batteries.

Despite certain progress in existing studies, there remain significant knowledge gaps: Firstly, most current research focuses on the modification effects of single membrane matrices, lacking systematic comparison of SiO_2's mechanism of action and insufficient elucidation of the structure-performance relationship between SiO_2 content and membrane pore structure, hydrophilicity, as well as bifunctional properties [4]. Secondly, regarding synergistic regulation of antifouling and anti-compaction performance, existing studies primarily emphasize optimization of individual properties, with inadequate investigation into microscopic mechanisms (e.g., effects of pore structure and particle dispersion) for their coordinated enhancement [6,13]. Thirdly, consensus has not been reached in literature regarding the optimal SiO_2 concentration that balances hydrophilicity, porosity, and mechanical stability, while the influence mechanisms of particle agglomeration at high SiO_2 contents require further detailed analysis [10,13]. For instance, Gaur et al.'s [10] TEM analysis revealed that SiO_2 concentrations exceeding 5 wt% tend to cause nanoparticle agglomeration, pore blockage, and structural defects, whereas Senol-Arslan et al. [4] identified 2 wt% SiO_2 as the optimal dosage for PVDF and PSF membranes,

Table 1
Key Literature Background on PVDF/SiO_2 membranes.

Study	Method	SiO_2 loading	Key findings	Limitations
Cui et al. (2010)[6]	TIPS	Micro-SiO_2	Maxium tensile strength (14.3 MPa) at 2 wt%; flux peaked at 70 $L{\cdot}m^{-2}{\cdot}h^{-1}$ (5 wt%)	No antifouling and anti-compaction studies
Liang et al. (2014)[14]	TIPS + sol–gel	Varied dosage of SiO_2 hydrolyzed from tetraethoxysilane via sol–gel	Contact angle decrease from 131° to 101°; improved flux & compaction resistance	Limited mechanical stability data
Wang et al. (2016) [12]	NIPS	SiO_2-g-PDMS	Enhanced antifouling & flux recovery; hierarchical pore structure	Limited mechanical stability data
Boateng (2018) [16]	TIPS	PVDF-co-HFP/SiO_2	Reduced polarization in batteries; high cyclability	Focused on energy storage, not water treatment
Amani et al. (2023) [13]	NIPs	Cu-SiO_2	Contact angle(CA) decreases by 20.70%; Porosity increases by 18.24%; Pure water flux(PWF) increases by 63.33%; The irreversible fouling ratio of neat PVDF and modified PVDF is 45.39% and 11.27%, respectively	Treating activated
M. Ahsani et al. (2020) [11]	NIPs	Ag-SiO_2	PWF of the nanocomposite PVDF membrane (PVDF/Ag-SiO_2; 0.6 wt%) increased by 60%; Water contact angle decreased from about 99° to 89°; Flux recovery ratio increased from 58% for the neat PVDF membrane to 76% for the nanocomposite PVDF/Ag-SiO_2 membrane; The chemical oxygen demand (COD) and ammonium removal efficiencies of the neat and nanocomposite membranes were higher than 90% and 95%	Lack knowledge on anticompaction data; Treating real pharmaceutical wastewater
Safamia et al. (2021) [7]	NIPs:dipping the PVDF/ polydopamine membrane in the soultion of Tetraethoxysilane	PVDF/polydopamine/silica membrane	CA of PVDF and hybrid membrane is 87 and 69, respectively; The permeability of PVDF and hybrid membrane is 9.5 and 2.6 9.5 $L/(m^2{\cdot}h{\cdot}bar)$, espectively; A rejection of 81.5% and of 91.6% for PVDF and hybrid membrane respectively;	Silica is on the film surface and can not take part in the formation process of membrane; Dealing with diclofenac waste water; no anti compression properties data
Kusworo et al. (2024) [17]	Sol-gel	GO-NiFe@SiO_2/PVDF	61.32% cleaning efficiency under UV irradiation; Dye decolorization rates of up to 90.50% alongside a moderate permeate flux reaching 30.46 $L{\cdot}m^{-2}{\cdot}h^{-1}$; Outstanding flux recovery, reaching up to 92.57%	Treatment of Dyeing Wastewater; No research on its anti compressive performance ; Using photocatalytic degradation function of nanoparticles
This work	TIPS	Nano-SiO_2	CA decreases by 14.27%; PWF increases by 268.93% to 233.9 $L{\cdot}m^{-2}{\cdot}h^{-1}$; Anti-compaction property is enhanced, and compaction rate decreases by 24.9%; The R_{ir} of PS3.0 and neat PVDF membrane is 0.33 m^{-1} and 6.52 m^{-1}, respectively	——

highlighting that SiO_2 content regulation must be comprehensively determined based on membrane fabrication methods and application scenarios. The key literature background on PVDF/SiO_2 membranes is summarized in Table 1.

To address the aforementioned research gap, this study employs the TIPS method to prepare PVDF/SiO_2 composite membranes and systematically investigates the effect of nano-SiO_2 content within the range of 0–6 wt% on membrane performance. The focus is on elucidating the intrinsic mechanisms by which SiO_2 concentration regulates membrane morphology, wettability, hydraulic performance, and antifouling-anticompaction behavior. Membrane morphology and properties are characterized using scanning electron microscopy (SEM), transmission electron microscopy (TEM), and contact angle measurements. Bovine serum albumin (BSA) is used as a model foulant, combined with long-term flux stability tests, to evaluate the practical application potential of the membranes. This study aims to establish correlations between SiO_2 content and membrane structure-performance relationships, providing theoretical insights for developing high-performance PVDF membranes suitable for harsh conditions such as high-pressure water treatment.

2. Experimental

2.1. Materials

PVDF (FR-904, number-average molecular weight Mn = 380,000, polydispersity index PDI = 1.7) was purchased from Shanghai 3F New Materials Co., Ltd.; nano SiO_2 (HN-2, particle size 10–30 nm, uncoated) was obtained from Zibo Haina New Materials Co., Ltd.; dimethyl phthalate (DMP) was sourced from Shanghai Bio Life Science & Technology Co., Ltd.; bovine serum albumin (BSA) was acquired from Sigma-Aldrich. All BSA solutions used in the experiments were freshly prepared and utilized within 8 h.

2.2. Preparation of hybrid membranes

Both the neat PVDF membrane and the PVDF/SiO_2 hybrid membrane were prepared using TIPS method. The detailed steps are provided in Supplementary File 1. The liquid mixture were prepared with PVDF powder and dilute with or without SiO_2 nano-particles. The dilute and SiO_2 mixture should be ultrasonically homogenized for 10 min before PVDF addition for PVDF/SiO_2 hybrid membrane preparation. Then the mixture was heated to 473 ± 5 K for 4 h and quenched in an ice-water bath to form the a solid polymer-diluent blend. The smashed blend was heated in a custom steel mold to 473 again, pressed and quenched. The flat sheet membranes were obtained after the diluent in the blend was extracted out by ethanol and dried.The specific compositions of the membranes are listed in Table 2.

2.3. Characterization of hybrid membranes

The surface and cross-section morphologies of the membranes were observed using a JEOL JEM-6700F SEM and a FEI Phenom Deskcope SEM. TEM observations were conducted with a JEOL JEM-2010 TEM. The pure water flux (*PWF*) and BSA retention properties of the fabricated membranes were evaluated using a cross-flow filtration experimental apparatus [17]. Membrane porosity was determined using the dry-wet method [6]. Contact angle (*CA*) measurements were performed using a contact angle meter (JYSP-180, Beijing). The pore size distribution was calculated using the liquid–liquid displacement method. Fouling experiments were conducted in accordance with the methodology outlined by Kang et al. [18]. The fouling experiment with the BSA solution was also analyzed using the fouling models proposed by Ho et al. [19] and Hermia et al. [20]. The tensile strength and elongation at break of the membrane were measured using a universal electronic tensile testing machine (AGS-J, Shimadzu). Detailed procedures for all experiments are provided in Supplementary file 2.

Table 2
Composition of the blends.

Membranes	PVDF (wt%)	SiO_2 (wt%)	DMP (wt%)
PS–0	30	0	70
PS–1.5	28.5	1.5	70
PS–3.0	27	3.0	70
PS–6.0	24	6.0	70

3. Results and discussion

3.1. Morphology studies

Fig. 1 presents cross-sectional SEM images of composite membranes with different SiO_2 contents. It can be observed that when the SiO_2 content ranges from 0 to 6 wt%, all membranes exhibit typical blurred spherulitic structures, indicating the occurrence of solid–liquid (S-L) phase separation. The spherulite size initially decreases progressively with increasing SiO_2 content,. The PS-3.0 membrane displays the smallest and most uniformly distributed spherulites as shown in Fig. 1 (c). However, it can be seen in Fig. 1(d) that significant SiO_2 agglomeration occurs when the SiO_2 content reaches 6 wt% (PS-6.0), which inhibits spherulite growth and results in irregular spherulite sizes.

SiO_2 particles, acting as heterogeneous nucleation agents, significantly influence the crystallization process of PVDF [9]. The nucleation time of neat PVDF membranes is affected by molecular weight, system temperature. and early-formed nuclei growing into large-sized crystals. However, uniformly dispersed SiO_2 particles increase the nucleation density, resulting in similar diffusion distances for PVDF molecules to adjacent nuclei, thereby forming spherulites with uniform sizes. Sufficient PVDF molecules are available, leading to similar cross-sectional structures in the membrane when the SiO_2 content is below 3.0 wt%, as shown in Fig. 1(a)-Fig. 1(b). While the amount of PVDF molecules becomes insufficient to form large crystals at the SiO_2 dosage of 3.0 wt%, resulting in the smallest spherulite size in Fig.(c). At the SiO_2 dosage of 6 wt%, SiO_2 agglomerates and the lack of PVDF molecules hinders crystal growth, forming irregular spherulitic structures in Fig. 1(d).

Fig. 2 presents the SEM images of the membrane surface. The membrane surface exhibits distinct spherulitic structures when the SiO_2 content ranges from 0 to 6 wt%. These spherulites display truncated morphologies due to their two-dimensional growth during phase separation while in contact with the steel substrate [21]. As the SiO_2 concentration increases from 0 to 3 wt%, both the spherulite size and interspherulitic voids decrease, accompanied by increased spherulite density and more uniform distribution, indicating that SiO_2 particles can suppress macrovoid formation between spherulites on the membrane surface in Fig. 2(a)-2(c). At 6 wt%, local irregular arrangements of surface spherulites occur due to particle agglomeration, though the spherulite-dominated structural characteristic remains preserved in Fig. 2(d). At low concentrations, nano-SiO_2 acts as a nucleating agent promoting crystallization. Whereas at high concentrations (6 wt%), SiO_2 agglomeration hinders crystallization——a phenomenon consistent with findings reported by Cui et al. [6] and Li et al. [23].

TEM images (Fig. 3) further confirmed the dispersion state of SiO_2 within the PVDF matrix. With increasing SiO_2 content, particle agglomeration became more pronounced: uniform dispersion was observed in Fig. 3(b) below 1.5 wt%, relatively good dispersion maintained at 3 wt% in Fig. 3(c), while significant micron-scale agglomerates formed at 6 wt% in Fig. 3(d). These agglomerates hindered the mobility of PVDF molecular chains, resulting in irregular spherulite morphology in the PS-6.0 membrane in Fig. 3(d).

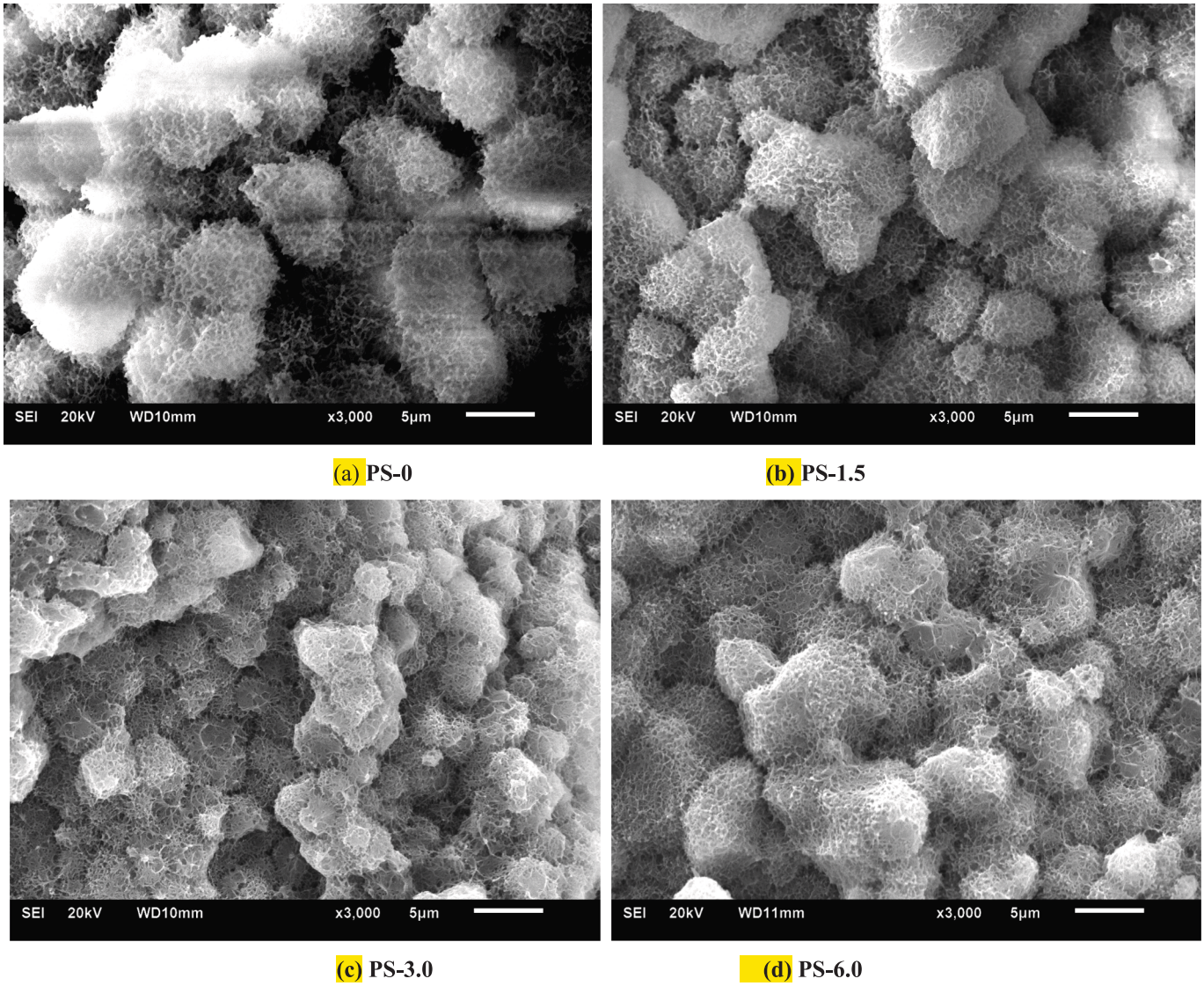

Fig. 1. SEM image (3000×) of the cross–section of hybrid membranes prepared with different SiO_2 dosages.

3.2. Pore size distribution

Fig. 4 presents the pore size distribution curves of composite membranes with different SiO_2 contents. The pore distribution curve of PS-0 is unimodal and exhibits a broad distribution of 175–365 nm with the optimal pore size of 295 nm, indicating non-uniform spherulite dimensions. When the SiO_2 content increases from 1.5 wt% to 3 wt%, the optimal pore size shifts to 24.4 and 22.25 nm with a narrow pore size distribution, demonstrating significantly improved pore size uniformity, which corresponds to the SEM observation of reduced and more concentrated spherulite sizes. At 6 wt% SiO_2 loading, the optimal pore size becomes 79.46 nm. The pore size distribution curves of PS-1.5, PS-3.0 and PS-6.0 all have three peaks. The second and the third peaks in the PS-1.5 and PS-3.0 closely link together, and in the PS-6.0 are far apart, showing decreased pore size uniformity. This phenomenon aligns with the TEM observation of SiO_2 agglomeration, where aggregated particles induce irregular pore structures forming multi-scale pores. The SiO_2 content governs the evolution of pore size distribution by regulating phase separation mechanisms and spherulite growth: At low concentrations (1.5–3 wt%), SiO_2 is uniformly dispersed as a nucleating agent, refining the spherulites and forming uniform fine pores; at high concentrations (6 wt%), particle aggregation disrupts the uniform growth of spherulites, leading to broadened pore size distribution and consequently affecting the membrane's separation efficiency[17,24].

3.3. Contact angle and wettability

The contact angle (CA) and its variation rate are key indicators for evaluating membrane wettability. As shown in Fig. 5, the CA of composite membranes continuously decreases with increasing SiO_2 content: the neat PVDF membrane exhibits a CA of 107.9°, which decreases to 98.6° at 1.5 wt%, further reduces to 95.2° at 3 wt%, and finally reaches 92.5° at 6 wt%. It demonstrates that the incorporation of SiO_2 significantly reduces the hydrophobicity of the membrane surface compared with neat PVDF membrane, which can be attributed to the enhanced interaction between the membrane surface and water molecules caused by hydroxyl (–OH) groups on the SiO_2 surface [7].

The variation rate of CA curves for the membranes is presented in Fig. 6. The CA change rate decreases from 0.76°/min of PS-0 to 0.736°/min. of PS-3.0, then increases again to 0.84°/min of PS-6.0 as the SiO_2 content increases from 0 to 6 wt%, different with the trend of CA changes. The wetting ability of the hybrid membrane is affected by membrane roughness, nature of the matrix, the surface tension,and the other parameters. It is reported that the batter scattered SiO_2 particles maybe an obstacles for water to diffusion path or channel for molecules, and kept the water drop on the membrane surface, while aggregated

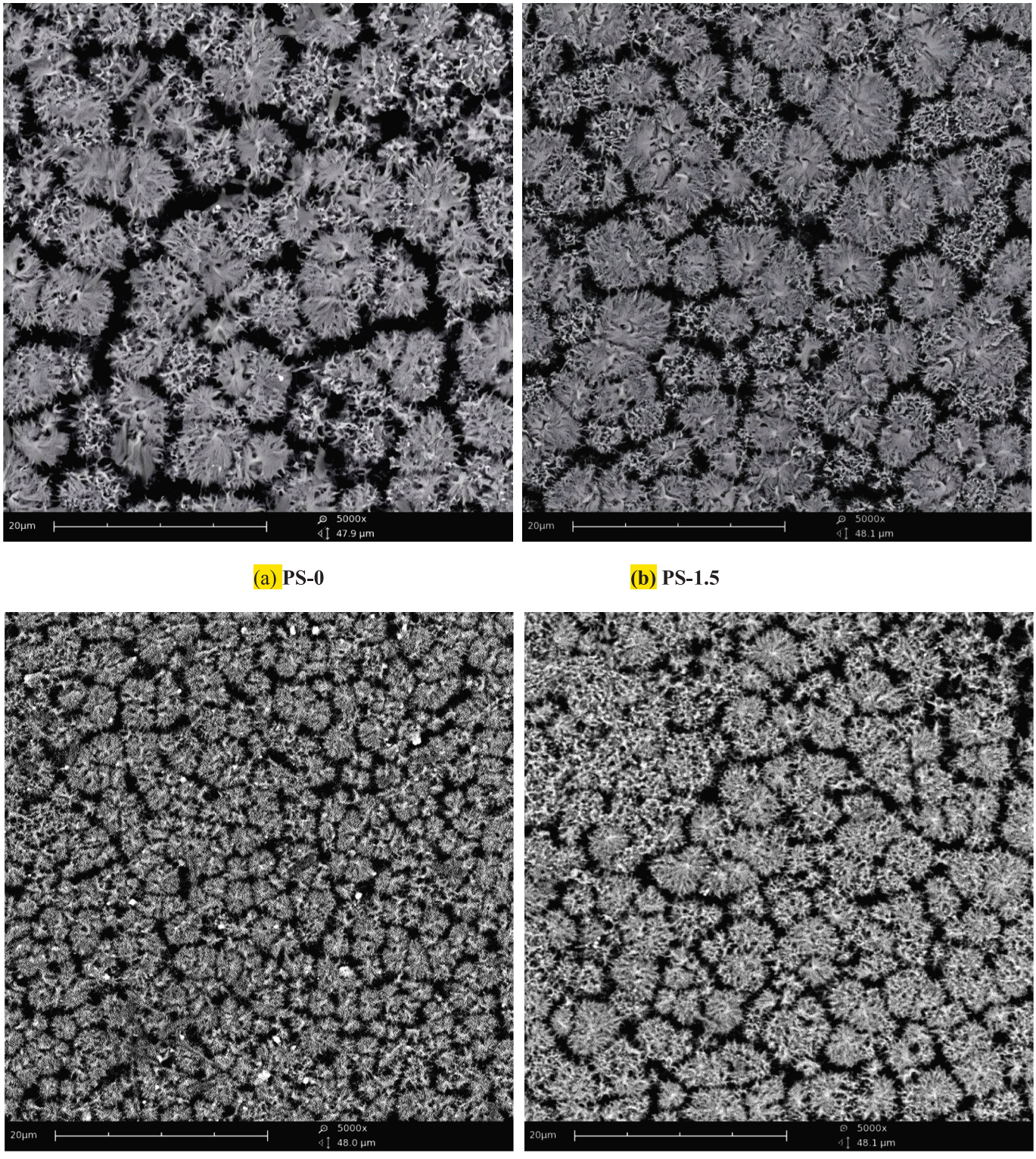

Fig. 2. SEM image (5000×) of the surface of hybrid membranes prepared with different SiO_2 dosages.

SiO_2 can act as channels for water through the membrane and accelerate the deformation of water drop[9]. In conjunction with Fig. 4, it can be observed that the rate of CA variation correlates with the membrane pore size. Water drops tends to pass through the pores of the membranes because of the influence of gravity. However, the surface tension of water causes it to form microspheres over the membrane surface, with the surface tension directed toward the center and upward. As long as the surface tension exceeds the gravitational force, water does not pass through the pore. The smaller the pore diameter, the greater the surface tension. Although neat PVDF membranes exhibit strong hydrophobicity, the rapid variation in their surface tension can be attributed to the fact that the surface tension of air within the spherulite gaps is insufficient to

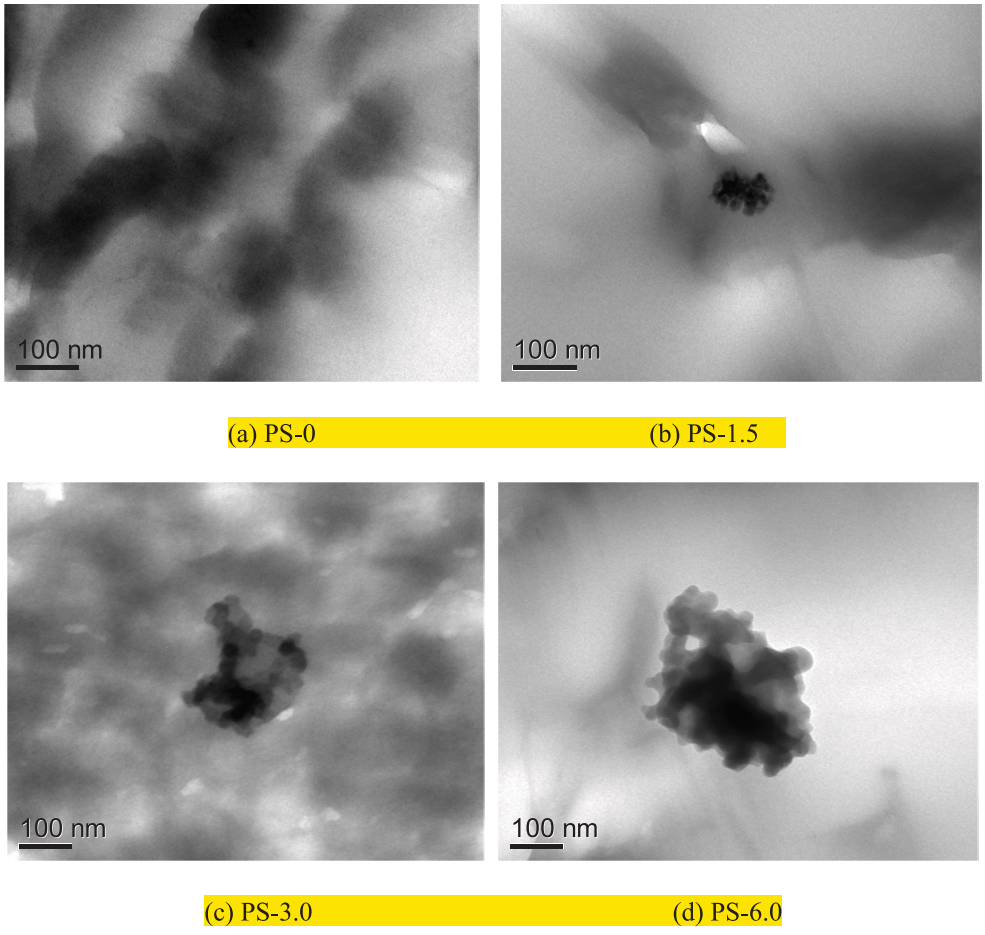

Fig. 3. Transmission electron micrographs (TEM) of PVDF/SiO_2 hybrid membranes with various SiO_2 dosages.

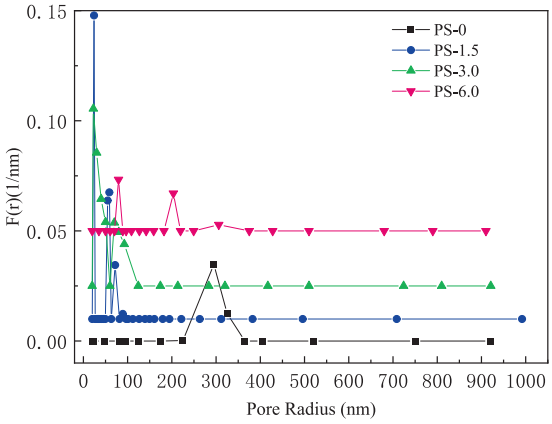

Fig. 4. Pore size distribution of PVDF/SiO_2 hybrid membranes with various SiO_2 dosages.

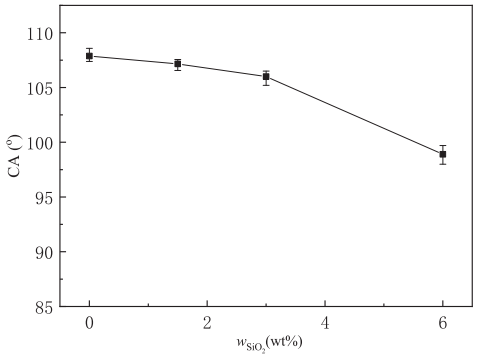

Fig. 5. *CA* of PVDF/SiO_2 hybrid membranes with different SiO_2 dosages.

support the weight of water droplets, resulting in rapid deformation of the droplets. Surface tension surpasses the hydrophilicity of SiO_2, enabling water droplets to maintain a perfect spherical shape. This is because as the silica content increases from 0 to 3 wt%, the pore size decreases, leading to slight deformation of the water droplets. However, with further increase in silica content, the pore size becomes larger again. Due to the combined effects of macropores and the hydrophilic nature of SiO_2, the contact angle of PS-6.0 undergoes rapid changes once more..

3.4. Porosity and PWF

Porosity is a critical factor influencing the pure water flux (PWF) of membranes, and generally, higher porosity leads to greater PWF. As shown in Fig. 7, the porosity of the hybrid membranes is 58.8%, 60%, 63.5%, and 67.3% at 0, 1.5, 3.0, and 6.0 wt% dosage of SiO_2. This phenomenon can be attributed to the formation of interfacial pores caused by interfacial stress between the polymer and SiO_2 particles during phase separation, thereby increasing the overall porosity. Compared with PVDF/TiO_2 composite membranes [25], PVDF/SiO_2 composite membranes exhibit significantly higher porosity under identical nanoparticle loading. For instance, at 3.0 wt%, the porosity of the PVDF/SiO_2 membrane (63.5%) is substantially higher than that of the

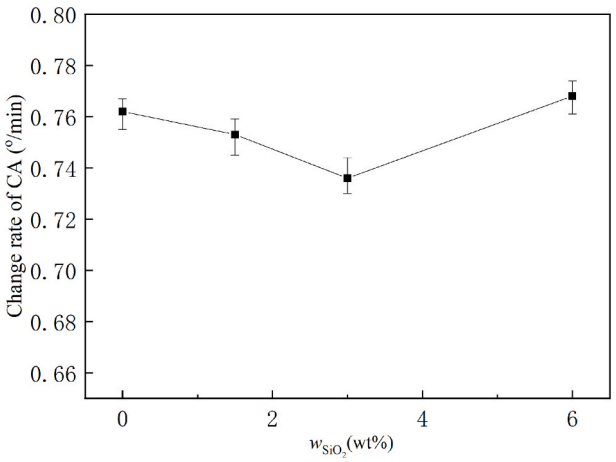

Fig. 6. Wetting ability of PVDF/SiO_2 hybrid membranes with different SiO_2 dosages.

PVDF/TiO2membrane (49.6%). It can be seen from the TEM picture of this paper and our previous paper [25]. The SiO_2 particles distributed more evenly in PVDF matrix than TiO_2 nanoparticles did at the same dosage. It hints the better compatibility between SiO_2 and the PVDF matrix, resulting in more pronounced heterogeneous nucleation effects and more porosity[17]. Meanwhile, the TiO_2 agglomerations stuck in the pores and decreased the porosity.

Fig. 8 demonstrates that PWF increases with rising SiO_2 content. The corresponding PWF values are 63.4, 162.8, 210.2 and 233.9 $L{\cdot}m^{-2}{\cdot}h^{-}1$ at 0, 1.5, 3.0 and 6.0 wt%, respectively. As shown above, the introduction of SiO_2 simultaneously enhances both the porosity and hydrophilicity of the membrane, thereby significantly improving PWF. Under identical particle loading conditions, the PWF of PVDF/SiO_2 composite membranes far exceeds that of PVDF/TiO_2 membranes [25]. For example, at 3.0 wt%, the PWF of the PVDF/TiO_2 membrane is only 73 $L{\cdot}m^{-2}{\cdot}h^{-1}$. The CA of the PVDF/$SiO_2$ and PVDF/TiO_2 membrane at the same nanoparticle dosage of 3.0 wt% is 95.2℃ and higher than 105°, respectively[25]. High hydrophilicity coupled with high porosity led PS-3.0 having higher PWF than PVDF/TiO_2. The PVDF/SiO_2 membranes with 5 wt% of micro-SiO2particles and dibutyl phthalate (DBP) as dilute had the flux peaked at 70 $L{\cdot}m^{-2}{\cdot}h^{-1}$, less than the PVDF/$SiO_2$ hybrid membrane in this study. The differences may be due to the size of SiO_2 particles and the dilute. The PVDF and SiO_2 have better compatibility with DBP than DMP [6],.

Fig. 9 presents the variation curve of PWF over operation time under 200 kPa. It can be observed that at identical operation durations, PWF increases with higher SiO_2 content; during the initial operation stage, PWF declines sharply, with membranes containing higher SiO_2 concentrations exhibiting faster flux decline rates, similar with the performance of PVDF/Cu-SiO_2 fabricated via NIPS method [13]. Subsequently, the attenuation rate decelerates and gradually stabilizes. The initial flux decline is attributed to membrane deformation under pressure (Fig. 10). The compaction degree of neat PVDF membrane reaches 49.4%, while SiO_2 doping reduces this compaction effect due to enhanced compressive resistance imparted by SiO_2. The PS-3.0 membrane demonstrates optimal polymer concentration-SiO_2 content matching, forming finer spherulite structures with minimal compaction degree (37.1%), indicating that smaller spherulite structures improve compressive resistance. In contrast, the PS-6.0 membrane exhibits irregular spherulite structures caused by agglomeration, resulting in slightly higher compaction degree (39.8%) compared to PS-3.0, though still significantly lower than neat PVDF membrane. As shown in Supplementary File 3, the PS-3.0 membrane achieves the highest tensile strength (10.35 MPa) and elongation at break (36.1%), further confirming its superior mechanical stability at this composition ratio.

Based on Eq. S8, the R_m of membrane samples was calculated. The absence of foulants in the liquid resulted in R_c and R_{ir} being considered zero, thus $R_m = R_t$. Fig. 11 presents the variation curves of membrane R_m under different operating times ($R_t = R_m$ in the absence of contaminants). The R_m of all membranes increases with time, but the growth rates differ significantly: the PS-0 membrane exhibits the highest initial resistance and the fastest growth rate, indicating that the neat PVDF membrane structure is unstable under pressure; membranes containing SiO_2 demonstrate a pronounced dosage effect, where increasing SiO_2

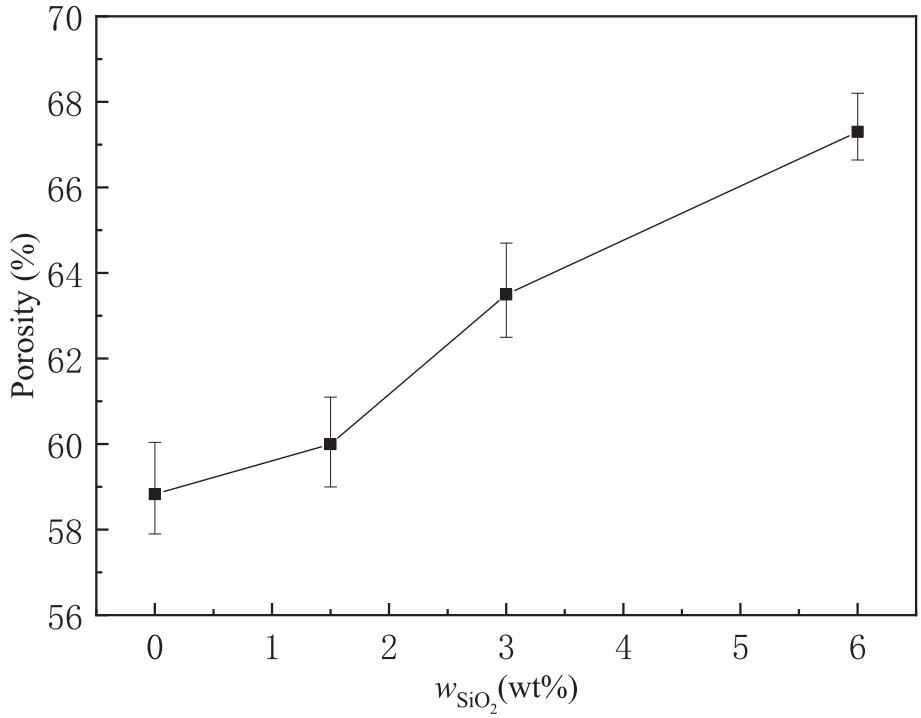

Fig. 7. Porosity of PVDF/SiO_2 hybrid membranes with different SiO_2 dosages.

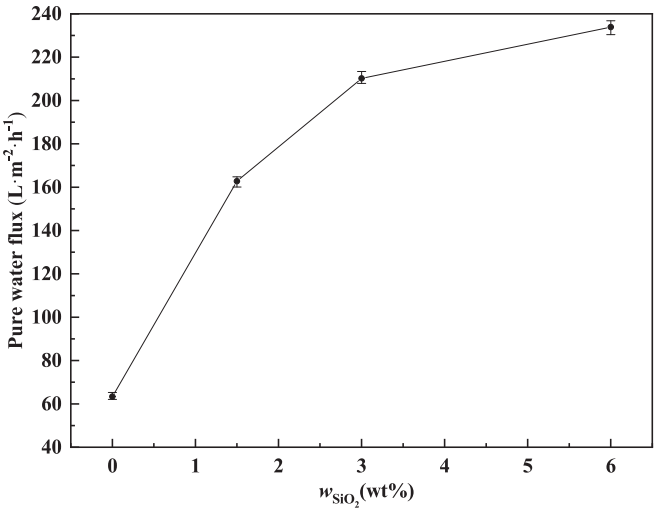

Fig. 8. PWF of PVDF/SiO_2 hybrid membranes at 0.1 MPa with different SiO_2 dosages.

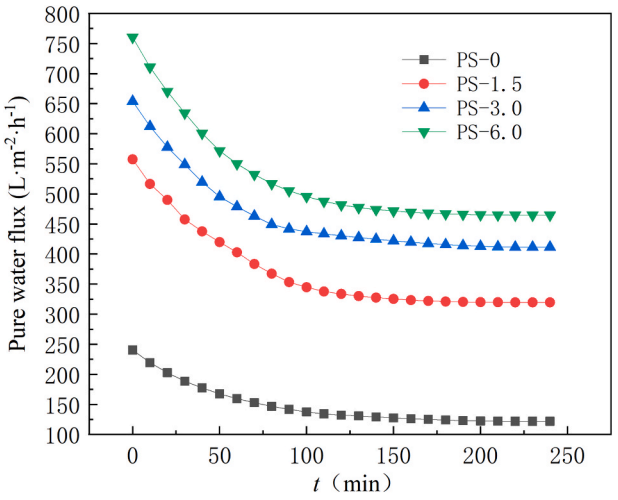

Fig. 9. *PWF* of PVDF/SiO_2 hybrid membranes with different SiO_2 dosages at different running time at 0.2 MPa.

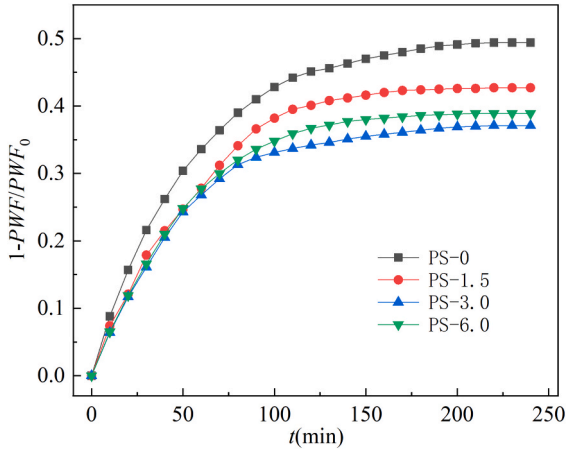

Fig. 10. The effect of SiO_2 dosage on the compaction degree of PVDF/SiO_2 hybrid membranes at different running time.

content reduces the initial Rm and significantly slows its growth rate. At

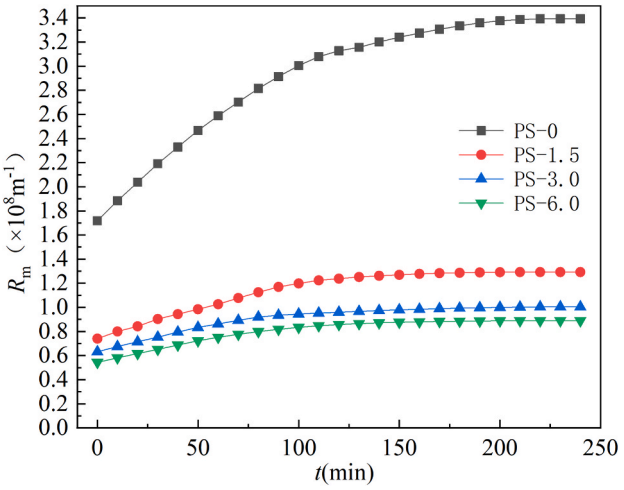

Fig. 11. The effect of SiO_2 dosage on the R_m (R_t) of PVDF/SiO_2 hybrid membranes at different running time.

3 wt%, R_m grows the slowest due to the uniformly dense spherulitic structure, which provides the strongest rigid support from SiO_2 particles; at 6 wt%, local structural defects caused by particle aggregation result in a slightly higher Rm growth rate compared to 3 wt%, though still substantially lower than that of the neat PVDF membrane. This indicates that the rigid support from SiO_2 particles can rapidly stabilize the membrane structure and mitigate pressure-induced deformation.

3.5. *Membrane fouling studies*

Fig. 12 shows the effect of SiO_2 content on BSA rejection rate. The BSA rejection rates of all composite membranes were below 20%, which was attributed to the insufficient membrane pore size for effectively retaining BSA molecules (particle size < 7 nm). The BSA rejection rate initially increased and then decreased with increasing SiO_2 content: from 8.7% for PS-0 to 12.6% for PS-3.0, followed by a decrease to 9.3% for PS-6.0, consistent with the changes in membrane pore size distribution. The PS-3.0 membrane exhibited the smallest and most uniform pore size, resulting in the highest rejection rate; whereas the PS-6.0 membrane showed enlarged pore sizes with broader distribution, allowing partial BSA molecules to pass through larger pores, thereby reducing the rejection efficiency.

Fig. 13 presents the filtration resistance analysis of composite membranes towards BSA solution. With increasing SiO_2 content, the total resistance (R_t), membrane resistance (R_m), cake layer resistance

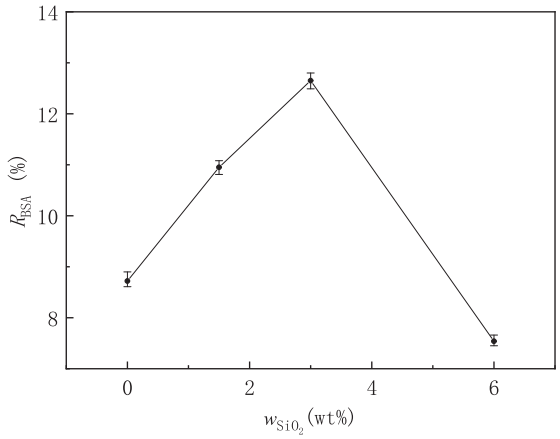

Fig. 12. Effect of SiO_2 content on BSA rejection of PVDF/SiO_2 hybrid membranes.

(R_c), and irreversible fouling resistance (R_{ir}) all decreased significantly. The PS-3.0 membrane exhibited the lowest resistance values: $R_t = 2.36$ m^{-1} and $R_{ir} = 0.33$ m^{-1}, representing reductions of 81.4% and 95.0%, respectively, compared to the neat PVDF membrane ($R_t = 12.73$ m^{-1}, $R_{ir} = 6.52$ m^{-1}). This improvement is attributed to SiO_2 enhancing membrane hydrophilicity, where surface –OH groups inhibited BSA molecule adsorption on the membrane surface. Simultaneously, the uniform pore structure reduced BSA blockage within the pores. For the PS-6.0 membrane, localized pore irregularities caused by agglomeration resulted in slightly higher R_{ir}(0.86 m^{-1}) compared to PS-3.0, but still significantly lower than the neat PVDF membrane. This indicates that even with minor agglomeration, the hydrophilic properties of SiO_2 remain effective in suppressing irreversible fouling.

The optimal pore size of the hydrophilic PVDF/SiO_2 membranes is smaller than 200 nm, and can be used to remove suspended solids, bacteria, parasite eggs, and large molecular organic matter in wastewater. For example, these membranes could be used to treat wastewater and activated sludge by submerged membrane bioreactor [13].

3.6. Fouling mechanism study

A 1000 ppm BSA solution was subjected to cross-flow filtration under a transmembrane pressure of 0.1 MPa, and the fouling mechanisms were analyzed through the relationship between d^2t/dV^2 and dt/dV (Fig. 14) using Hermia's fouling model [21]. The 0, 1, 1..5 and 2 of n in the Hermia's fouling model means the membrane fouled because of cake filtration, intermediate blockage, pore constriction and complete pore blockage, respectively[21].

During the initial filtration stage, the resistance growth rate exhibited a positive correlation with acceleration. The slopes (n, Supplementary file 4) of PS-0, PS-1.5, PS-3.0, and PS-6.0 were determined as 13.92, 8.55, 4.06, and 5.83, respectively. PS-0 demonstrated the fastest resistance increase accompanied by the highest peak acceleration, whereas PS-3.0 showed the slowest resistance development with the lowest peak acceleration, indicating superior antifouling performance of the PS-3.0 membrane. The hydrophobic surface of PS-0 promoted BSA adsorption and accumulation, resulting in rapid fouling kinetics. In contrast, the enhanced hydrophilicity and refined spherulite structure of PS-3.0 membrane reduced BSA adhesion, thereby improving antifouling capability. For PS-6.0 membrane, residual locally hydrophobic regions caused by particle aggregation facilitated preferential BSA adsorption, leading to a slightly higher resistance growth rate compared to PS-3.0.

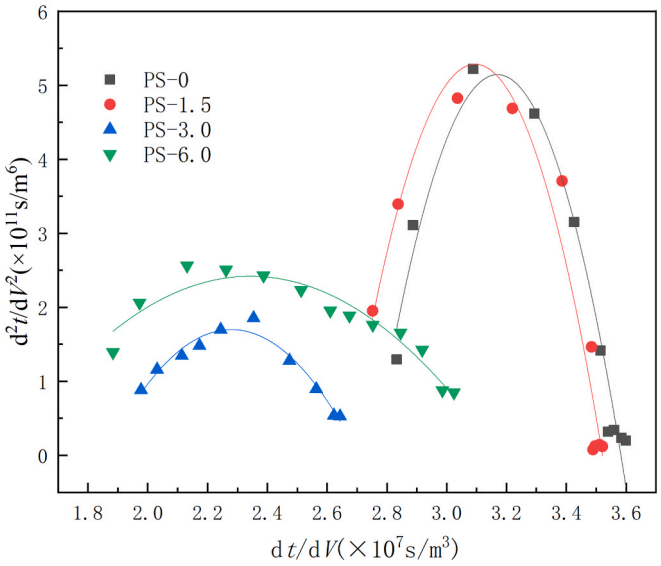

Fig. 14. The plot of $d^2t/dV^2 \sim dt/dV$ of PVDF/SiO_2 hybrid membranes.

At the later stage of the filtration process, the rate of resistance increase gradually diminishes and stabilizes with $n \approx 0$. According to Hermia's fouling model [21], this indicates that the fouling mechanism corresponds to cake layer filtration: contaminants (BSA) continuously accumulate on the membrane surface forming a dense cake layer, where

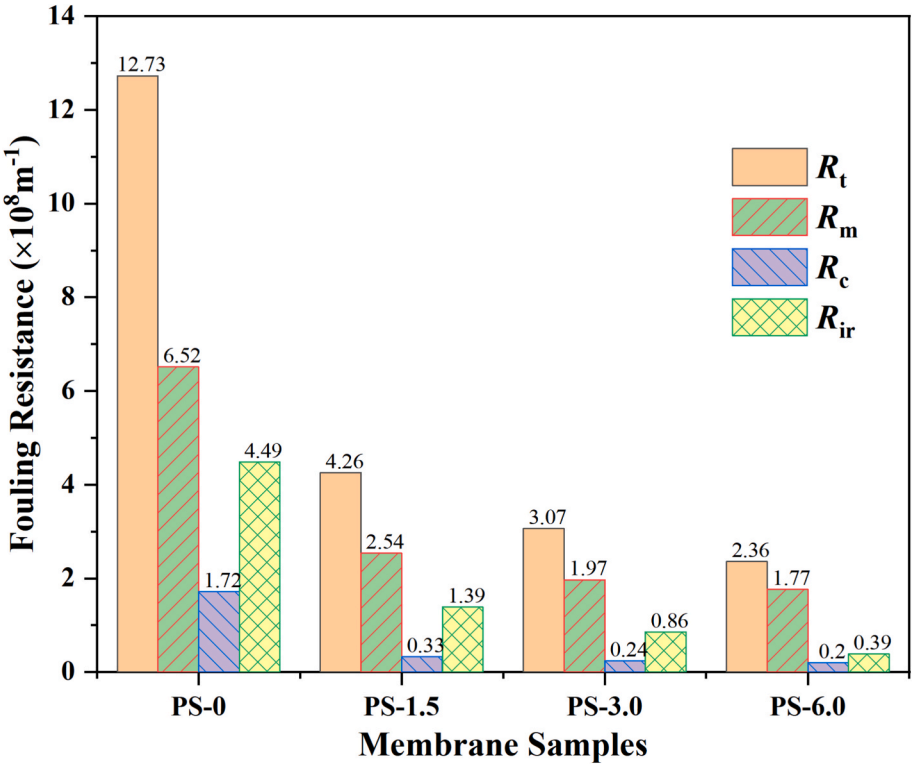

Fig. 13. Different filtration resistance of PVDF/SiO_2 hybrid membranes for BSA solution.

the cake layer resistance (R_c) increases linearly with time, resulting in uniform elevation of dt/dV ($d^2t/dV^2 \approx 0$). The SiO_2 content demonstrates regulatory effects on fouling behavior: At 3 wt%, enhanced hydrophilicity (contact angle 95.2°) and uniform pore structure reduce BSA adsorption, yielding the slowest cake layer formation rate; At 6 wt%, although hydrophilicity further improves, irregular pore structures caused by particle aggregation lead to localized cake layer accumulation, producing slightly faster formation kinetics than at 3 wt%; The pristine PVDF membrane exhibits rapid BSA adsorption and aggregation due to its hydrophobic surface and heterogeneous pore structure, resulting in the fastest cake layer formation rate among all samples.

3.7. Optimizing mechanism of SiO_2 dosage on anti-compaction and anti-fouling performance

3.7.1. The optimizing mechanism of SiO_2 dosage on membrane's anti-compaction performance

The doping of 3 wt% SiO_2 significantly optimizes the spherulitic structure of the membrane: SiO_2 acts as heterogeneous nucleation sites, refining the PVDF spherulite size (SEM reveals that PS-3.0 exhibits the smallest spherulites), and forming a uniform and dense microstructure (Fig. 1 and Fig. 4). This refined spherulitic structure demonstrates greater resistance to deformation under pressure and superior mechanical stability, with a deformation rate of only 37.1% for PS-3.0, which is much lower than the 49.4% observed in neat PVDF membranes. Meanwhile, SiO_2 particles, as rigid fillers dispersed within the polymer matrix, form a rigid network that inhibits the slippage of PVDF chain segments within the spherulitic structure, further enhancing antifouling performance. This is evidenced by the slowdown in the growth rate of membrane resistance (R_m) with increasing SiO_2 content (Fig. 11).

At 6 wt% SiO_2, particle aggregation disrupted the uniformity of the spherulitic structure and caused localized irregular pores, resulting in a compaction degree (39.8%) slightly higher than that at 3 wt%, but still significantly lower than that of neat PVDF membranes. This indicates that the rigid support effect of SiO_2 remains dominant; even with minor aggregation present, it can still effectively suppress irreversible deformation of the membrane.

3.7.2. The optimizing mechanism of SiO_2 dosage on membrane's anti-fouling performance

Enhancement of hydrophilicity: The hydroxyl groups (–OH) on the SiO_2 surface significantly reduce the contact angle from 107.9°, as observed in neat PVDF, to 92.5° when 6 wt% SiO_2 is incorporated (Fig. 5). This increased hydrophilicity leads to a decreased adsorption of hydrophobic foulants such as BSA and results in a substantial reduction (>60%) in the R_{ir} (Fig. 13).

Mechanism of fouling transition: The introduction of SiO_2 optimizes membrane pore size, achieving a uniform pore size distribution between 20–150 nm at 3 wt%, which reduces blockage of pores by contaminants (Fig. 4). The Hermia model confirms that the fouling of the composite membrane is predominantly governed by a reversible cake layer. The hydrophilic surface inhibits tight adsorption of BSA, enabling rapid flux recovery through physical cleaning alone (flux recovery rate > 90%). At 6 wt%, some larger pore channels allow easier passage of BSA, resulting in a slightly faster formation rate of the cake layer; however, the reversibility remains intact, with a flux recovery rate exceeding 85%.

Regulation of fouling resistance distribution: The synergistic effect of hydrophilicity and high porosity(PS-3.0 and PS-6.0) effectively mitigates pore blockage (Fig. 13).

In summary, SiO_2 enhances the performance of PVDF membranes via a threefold mechanism: (1) Structural reinforcement: The incorporation of nanoparticles refines the structure of the spherulites, thereby improving their mechanical stability; (2) Hydrophilic modification: The presence of hydroxyl (–OH) groups inhibits the adsorption of pollutants; (3) Pore regulation: The uniformity of pore size minimizes clogging, which in turn facilitates reversible fouling. The optimal SiO_2 content is determined as 3 wt%, while a 6 wt% concentration exhibits slight performance deterioration due to particle aggregation but remains superior to pristine PVDF membranes. It reveals that the amount of SiO_2 enables directed design of the membrane's microstructure by regulating phase separation pathways and spherulite growth, providing high-performance PVDF-based composite membrane materials for demanding applications such as high-pressure water treatment. This study provides critical insights for designing membrane materials applicable in high-pressure water treatment systems.

4. Conclusions

SiO_2 doping (0–6 wt%) effectively modulates the anti-compaction and anti-fouling performance of PVDF membranes, thereby enhancing their overall performance. This enhancement is primarily evident in several key areas:

1) The PVDF/ SiO_2 membranes with 0 to 6 wt% dosage of SiO_2 underwent S-L phase separation with the smallest spherulites and uniform pores at the dosage of 3 wt%.

2) Embedding SiO_2 nanoparticles into PVDF matrix can enhance hydraulic properties of hybrid membranes: CA decreases from 107.9° to 92.5°. Porosity and PWF improved by 19.7% and by 269.0% with the SiO_2 dosage increase from 0 to 6 wt%.

3) The SiO_2 nanoparticles with the dosage of 3 wt% endows the hybrid membrane maximum compaction resistance (37.1% deformation vs. 49.4% for neat PVDF), with tensile strength and elongation at break reaching 10.35 MPa and 36.1%, respectively.

4) PVDF/ SiO_2 hybrid membranes have decreased irreversible fouling (R_{ir} drops > 60%) and cake-layer fouling is the dominant fouling mechanism confirmed by Hermia model.

5) The optimal dosage was determined to be 3 wt% SiO_2, endowing hybrid membrane excellent pressure resistance, antifouling performance,anti-compression performance and high cleaning efficiency.

CRediT authorship contribution statement

Shuqi Ma: Writing – original draft, Validation, Methodology, Investigation, Funding acquisition, Data curation. **Fengmei Shi:** Writing – review & editing, Writing – original draft, Validation, Project administration, Methodology, Investigation, Funding acquisition, Formal analysis. **Boming Fan:** Writing – original draft, Validation, Methodology, Investigation, Formal analysis. **Qi Shen:** Validation, Methodology, Investigation, Formal analysis. **Jinglong Yuan:** Validation, Methodology, Investigation, Formal analysis, Data curation. **Chao Lin:** Validation, Methodology, Investigation, Data curation. **Yuxin Ma:** Writing – review & editing, Writing – original draft, Validation, Supervision, Methodology, Investigation, Funding acquisition, Formal analysis, Data curation, Conceptualization.

Declaration of competing interest

The authors declare that they have no known competing financial interests or personal relationships that could have appeared to influence the work reported in this paper.

Acknowledgments

This work was supported by National Natural Science Foundation of China (U21A20162), Heilongjiang Province Scientific and Technological Innovation Base Award Program (JD25B011), Heilongjiang Provincial Key Research Projects (2022ZXJ08B02), Basic Research Project of Scientific Research Funds for Universities in Heilongjiang Province (2024-KYYWF-0098) and National undergraduate innovation and entrepreneurship training program from Heilongjiang University

(202510212171S, 202410212095S).

Appendix A. Supplementary data

Supplementary data to this article can be found online at https://doi.org/10.1016/j.matdes.2026.115738.

Data availability

Data will be made available on request.

References

[1] S. Maiti, S.S. Islam, S. Bose, Nano-engineering for purity: advances in PVDF membrane water purification, ACES 20 (2025) e00788, https://doi.org/10.1002/asia.202500788.

[2] P.D. Sutrisna, K.A. Kurnia, U.W.R. Siagian, S. Ismadji, I.G. Wenten, Membrane fouling and fouling mitigation in oil-water separation: a review, J. Environ. Chem. Eng. 10 (2022) 107532, https://doi.org/10.1016/j.jece.2022.107532.

[3] P. Subasinghe, K.A.M. Said, M.R. Rahman, K.K. Kuok, Polyvinylidene fluoride gravity-driven membranes modification and membrane fouling: a review, Groundwater Sust. Dev. 26 (2024) 101215, https://doi.org/10.1016/j.gsd.2024.101215.

[4] D. Senol-Arslan, A. Gul, Enhancing oil rejection in PVDF and PSF membranes: the role of SiO_2 NPs, J. Appl. Polym. Sci. 142 (2025) 56590, https://doi.org/10.1002/app.56590.

[5] B. Ozbey-Unal, C. Balcik, B. van der Bruggen, Development of a novel hydrophilic SiO_2/PVDF Janus membrane via different modification methods for robust antiwetting and antifouling membrane distillation, J. Water Process Eng. 54 (2023) 104021, https://doi.org/10.1016/j.jwpe.2023.104021.

[6] A. Cui, Z. Liu, C. Xiao, Y. Zhang, Effect of micro–sized SiO_2–particle on the performance of PVDF blend membranes via TIPS, J. Membr. Sci. 360 (2010) 259–264, https://doi.org/10.1016/j.memsci.2010.05.023.

[7] M. Safarnia, M. Pakizeh, M. Namvar-Mahboub, Assessment of structural and separation properties of a PVDF/PD composite membrane incorporated with TiO_2 nanotubes and SiO_2 particles, Ind. Eng. Chem. Res. 60 (2021) 659–669, https://doi.org/10.1021/acs.iecr.0c06045.

[8] C. Wei, F. Dai, L. Lin, Z. An, Y. He, X. Chen, L. Chen, Y. Zhao, Simplified and robust adhesive-free superhydrophobic SiO_2-decorated PVDF membranes for efficient oil/water separation, J. Membr. Sci. 555 (2018) 220–228, https://doi.org/10.1016/j.memsci.2018.03.058.

[9] Y. Liu, J. Zhang, J. Li, Y. Zhao, M. Zhang, Impact of SiO_2 doping on the structure and oil-water separation properties of a PVDF membrane: insights from molecular dynamics simulation, RSC Adv. 14 (2024) 23910–23920. https://pubs.rsc.org/en/content/articlelanding/2024/ra/d4ra03807j.

[10] M.S. Gaur, A.P. Indolia, A.A. Rogachev, A.V. Rahachou, Influence of SiO_2 nanoparticles on morphological, thermal, and dielectric properties of PVDF, J. Therm. Anal. Calorim. 122 (2015) 1403–1416, https://doi.org/10.1007/s10973-015-4872-x.

[11] M. Ahsani, H. Hazrati, M. Javadi, M. Uibricht, R. Yegani, Preparation of antibiofouling nanocomposite PVDF/Ag-SiO_2 membrane and long-term performance evaluation in the MBR system fed by real pharmaceutical wastewater, Sep. Purif. Technol. 249 (2020) 116938, https://doi.org/10.1016/j.seppur.2020.116938.

[12] Q. Xu, Y. Chen, T. Xiao, X. Yang, A facile method to control pore structure of PVDF/SiO_2 composite membranes for efficient oil/water purification, Membranes 11 (2021) 803, https://doi.org/10.3390/membranes11110803.

[13] S. Amani, H.N. Kazerouni, S.M. Khiavi, A. Akbari, R. Yegani, Improving the antibiofouling and operational properties of PVDF membranes using synthesized Cu-SiO_2 nanoparticles in a submerged membrane bioreactor, Chem. Eng. Technol. 46 (2023) 2200–2207, https://doi.org/10.1002/ceat.202200576.

[14] H. Liang, Q. Wu, L. Wan, X. Huang, Z. Xu, Thermally induced phase separation followed by in situ sol-gel process: a novel method for PVDF/SiO_2 hybrid membranes, J. Membr. Sci. 465 (2014) 56–67, https://doi.org/10.1016/j.memsci.2014.03.068.

[15] L. Liu, Z. Wang, Z. Zhao, Y. Zhao, F. Li, L. Yang, PVDF/PAN/SiO_2 polymer electrolyte membrane prepared by combination of phase inversion and chemical reaction method for lithium ion batteries, J. Solid State Electrochem. 20 (2016) 699–712, https://doi.org/10.1007/s10008-015-3095-1.

[16] B. Boateng, G. Zhu, W. Lv, D. Chen, C. Feng, M. Waqas, S. Ali, K. Wen, W. He, An efficient, scalable route to robust PVDF-co-HFP/SiO_2 separator for long-cycle lithium ion batteries, Phys. Status Solidi RRL 12 (2018) 1800319, https://doi.org/10.1002/pssr.201800319.

[17] Y. Ma, F. Shi, J. Ma, M. Wu, J. Zhang, C. Gao, Effect of PEG additive on the morphology and performance of polysulfone ultrafiltration membranes, Desalination 272 (2011) 51–58, https://doi.org/10.1016/j.desal.2010.12.054.

[18] G. Kang, H. Yu, Z. Liu, Y. Cao, Surface modification of a commercial thin film composite polyamide reverse osmosis membrane by carbodiimide-induced grafting with poly(ethylene glycol) derivatives, Desalination 275 (2011) 252–259, https://doi.org/10.1016/j.desal.2011.03.007.

[19] C.-C. Ho, A.L. Zydney, A combined pore blockage and cake filtration model for protein fouling during microfiltration, J. Colloid Interface Sci. 232 (2000) 389–399, https://doi.org/10.1006/jcis.2000.7231.

[20] J. Hermia, Constant pressure blocking filtration laws-application to power-law non-newtonian fluids, Trans. Inst. Chem. Eng. 60 (1982) 18–37, https://doi.org/10.1080/01496398208055632.

[21] D.-J. Lin, K. Beltsios, C.-L. Chang, L.-P. Cheng, Fine structure and formation mechanism of particulate phase-inversion poly(vinylidene fluoride) membranes, J. Polym. Sci. Pol. Phys. 41 (2003) 1578–1588, https://doi.org/10.1002/polb.10513.

[22] X. Li, X. Lu, Morphology of polyvinylidene fluoride and its blends in thermally induced phase separation process, J. Appl. Polym. Sci. 101 (2006) 2944–2952, https://doi.org/10.1002/app.23489.

[23] T.D. Kusworo, N. Aryanti, A.M.A. Inamullah, D.A.P. Astuti, D.P. Utomo, Advanced photocatalytic membrane GO-NiFe@SiO2/PVDF for efficient decontamination of synthetic dyes in batik wastewater with superior antifouling features, J. Water Process Eng. 66 (2024) 105953, https://doi.org/10.1016/j.jwpe.2024.105953.

[24] T. Hou, X. Liu, J. Ren, X. Xu, D. Lan, S. Zhang, H. Guo, G. Wu, Z. Jia, G. Wu, Mesoporous hollow silica with controlled particle size for optimizing dielectric properties and coefficient of thermal expansion of polyimide packaging materials, Journal of Materials Science & Technology 235 (2025) 122–132, https://doi.org/10.1016/j.jmst.2025.03.014.

[25] F. Shi, Y. Ma, J. Ma, P. Wang, W. Sun, Preparation and characterization of PVDF/TiO_2 hybrid membranes with different dosage of nano-TiO_2, J. Membr. Sci. 389 (2012) 522–531, https://doi.org/10.1016/j.memsci.2011.11.022.